Temperature relaxation in strongly-coupled binary ionic mixtures

Robert Sprenkle
Brigham Young University
Luciano Silvestri
Michigan State University
M. S. Murillo
Michigan State University
Scott Bergeson (scott.bergeson@byu.edu)
Brigham Young University https://orcid.org/0000-0002-3124-9226

Article

Keywords: plasma science, high-energy-density (HED) systems

Posted Date: February 8th, 2021

DOI: https://doi.org/10.21203/rs.3.rs-159714/v1

Version of Record: A version of this preprint was published at Nature Communications on January 10th, 2022. See the published version at https://doi.org/10.1038/s41467-021-27696-5.

Temperature relaxation in strongly-coupled binary ionic mixtures

R. Tucker Sprenkle[1], L. G. Silvestri[2], M. S. Murillo[2], S. D. Bergeson[1]

[1]Department of Physics and Astronomy,
Brigham Young University, Provo, UT 84602, USA
[2]Department of Computational Mathematics, Science and Engineering,
Michigan State University, East Lansing, MI 48824, USA

New facilities such as the National Ignition Facility and the Linac Coherent Light Source have pushed the frontiers of high energy-density matter. These facilities offer unprecedented opportunities for exploring extreme states of matter, ranging from cryogenic solid-state systems to hot, dense plasmas, with applications to inertial-confinement fusion and astrophysics. However, significant gaps in our understanding of material properties in these rapidly evolving systems still persist. In particular, non-equilibrium transport properties of strongly-coupled Coulomb systems remain an open question. Here, we study ion-ion temperature relaxation in a binary mixture, exploiting a recently-developed dual-species ultracold neutral plasma. We compare measured relaxation rates with atomistic simulations and a range of popular theories. Our work validates the assumptions and capabilities of the simulations and invalidates theoretical models in this regime. This work illustrates an approach for precision determinations of detailed material properties in Coulomb mixtures across a wide range of conditions.

Introduction

Advancing the frontier of dense plasma science requires a deep understanding of plasma processes in extreme conditions. In laboratory experiments, these high-energy-density (HED) systems are transient – some lasting only a few microseconds (*1*). In laser-driven fusion experiments, for example, the target temperature changes from nearly absolute zero to millions of degrees. During this process, the target density increases by up to a factor of 1000. Minor imperfections in the target design or the laser wavefront drive instabilities that significantly change the maximum density and temperature (*2*).

Accurately modeling HED plasmas (HEDP) requires detailed and reliable models of collective phenomena such as continuum depression heating (*3*), turbulence and mixing (*4–6*), diffusion (*7, 8*), viscosity (*9*), and many other physical processes (*10, 11*). Representations of the Coulomb interaction (*12–14*) and the equations of state (*15*) are inherently uncertain across the extreme range of temperature and density, and add complexity to the modeling requirements. Stringent modeling needs are also found in stellar atmospheres (*16, 17*), a need that will become more acute as multi-messenger astronomy probes an increasingly rich diversity of transient plasmas.

An unsolved issue for predicting transport coefficients is determining how to treat strong, dynamical collision processes. When collisions are characterized by strong binary scattering events, cross sections in the Boltzmann equation accurately describe transport properties (*18*). Conversely, when collisions are characterized by weak many-body scattering events, dielectric functions in the Lenard-Balescu equation more appropriately describe transport (*19, 20*). However, when neither limit is realized, hybrid models are required (*21*). One approach is to build the many-body screening into an effective potential and to use it when computing cross sections, thereby capturing the strengths of both limits (*18, 22, 23*). To accurately represent experiments,

dense plasma models must include effects of Fermi degeneracy (*19*), atomic physics (*24*), and strong scattering (*25*). In different limits, these can manifest as coupled modes (*26–28*) or features of the pseudopotentials (*29*).

Because most plasmas are created out of equilibrium, understanding temperature relaxation is critical for modeling the evolution of multi-temperature high energy-density plasmas (*30–35*). Temperature relaxation has been studied extensively for electron-ion systems (*19,20,25–28,36–39*) and plasma theories are tailored for the case of disparate mass. These theories have been compared to molecular dynamics (MD) simulations with varying degrees of success (*37, 39*). Explicit electron-ion MD simulations often rely on quantum statistical potentials (*12,40*) which may only be valid in thermodynamic equilibrium (*36*). To avoid these problems, fictitious charges (*22, 38*) or alternate techniques (*41, 42*) are sometimes used.

It is desirable to employ a surrogate experiment at lower density and temperature, in which the density, temperature, and ionization states of the individual species are known, with diagnostics specific to the component process under consideration (*11*). In such a HEDP simulator, it is possible to test collision physics without the complications of high density, inaccessibly short time scales, high transient pressures, and extreme optical opacity.

Recent laboratory experiments have shown ultracold neutral plasmas (UNPs) to be effective HEDP simulators over a limited range of parameters (*11, 43–50*). In these strongly-coupled, non-degenerate, quasi-homogeneous, quasi-steady-state plasmas the charge state is well-known, the initial electron temperature, independent of the ion temperature, is chosen with sub-percent accuracy, and the time-evolving temperatures and densities of each ion species are readily determined. Furthermore, the equation of state is well known, dramatically reducing the complexity of interpreting experimental data and applying plasma models (*51*).

In this paper we report the first measurements of the ion-ion temperature relaxation rate using a strongly-coupled dual-species UNP (*46*). This system allows precise control of the

ion mass ratio and plasma stoichiometry. We show that within the experimental uncertainties, the measured temperature relaxation rates match the results of classical MD simulations. The same sign of charge removes ambiguities in the choice of the potential discussed previously. We compare rates extracted from these simulations with theoretical predictions in the few cases where the mass ratio dependence can be readily identified. We find reasonably good agreement with a recent model based on an effective Boltzmann equation (*52*).

Methods

Theoretical Considerations

We consider a spatially homogeneous plasma composed of two ion species with different masses, m_α, different number densities, n_α, and charge numbers, Z_α. The surrounding negative electronic background is at temperature T_e and density $n_e = Z_1 n_1 + Z_2 n_2$. The Wigner-Seitz radius is defined from the total ion number density, $a_{\rm ws}^3 = 3/4\pi n_{\rm tot}$, $n_{\rm tot} = n_1 + n_2$. The concentration of each ion species is $x_\alpha = n_\alpha / n_{\rm tot}$. Notice that $n_e = n_{\rm tot}$ when $Z_1 = Z_2 = 1$. The ion Debye length of species α is $\lambda_\alpha^2 = \epsilon_0 k_B T_\alpha / (n_\alpha (Z_\alpha e)^2)$. The ion plasma frequency of species α is $\omega_\alpha^2 = (Z_\alpha e)^2 n_\alpha / (\epsilon_0 m_\alpha)$. The total ion plasma frequency is $\omega_p^2 = \sum_\alpha \omega_\alpha^2$. We further define an average temperature as

$$T_{\rm avg} = \frac{m_\alpha T_\beta + m_\beta T_\alpha}{m_\alpha + m_\beta}, \tag{1}$$

and the ion thermal speed of species α is given by $v_{\alpha,\rm th} = \sqrt{k_B T_\alpha / m_\alpha}$. The strong coupling plasma parameter of species α is defined as

$$\Gamma_\alpha = \frac{(Z_\alpha e)^2}{4\pi\epsilon_0 a_{\rm ws}} \frac{1}{k_B T_\alpha}. \tag{2}$$

Typical equilibrium values in our experiments are $\Gamma_\alpha = 3$.

In a spatially homogeneous plasma with two ion species collisional temperature relaxation

(*53*) is described as

$$\frac{dT_\alpha}{dt} = -\nu_{\alpha\beta}(T_\alpha - T_\beta), \tag{3}$$

where α, β refer to different ion species. The collision frequency $\nu_{\alpha\beta}$ depends critically on temperature, density, and charge. In general, the collision frequencies can be represented as

$$\nu_{\alpha\beta} = n_\beta \Phi \mathcal{S}, \tag{4}$$

where

$$\Phi = \left(\frac{Z_\alpha Z_\beta e^2}{4\pi\epsilon_0}\right)^2 \frac{\sqrt{m_\alpha m_\beta}}{(m_\alpha + m_\beta)^{3/2}} \left(\frac{1}{k_B T_{\rm avg}}\right)^{3/2}, \tag{5}$$

is a reduced collision cross section and $\mathcal{S}$ is a model-dependent collisional integral.

Most treatments of temperature relaxation focus on electron-ion systems with the electron temperature much higher than the ion temperature. Few of these theoretical results can be applied directly to the case of ion-ion relaxation when the mass ratio is near unity. However, in the following we discuss ion-ion temperature relaxation rates derived from three models with increasing fidelity.

The first model is found in the NRL Plasma Formulary (*54*), p. 33. This model is based on the Fokker-Planck equation that leads to the well known Coulomb Logarithm (CL), $\mathcal{S} = \lambda_{\alpha\beta}$. In strongly-coupled plasmas, $\lambda_{\alpha\beta}$ is negative and needs to be modified.

A treatment based on hyperbolic trajectories (*25*) yields a positive definite result and takes the form

$$\mathcal{S}^{\rm NRL} = \frac{1}{2} \ln\left[1 + \left(\frac{b_{\rm max}}{b_{\rm min}}\right)^2\right], \tag{6}$$

where

$$b_{\rm max} = \left(\frac{1}{\lambda_1^2} + \frac{1}{\lambda_2^2}\right)^{-1/2}, \tag{7}$$

$$b_{\rm min} = \left(\frac{Z_1 Z_2 e^2}{4\pi\epsilon_0}\right) \frac{1}{k_B T_{\rm avg}}. \tag{8}$$

Equation (6) gives the NRL result in the limit of large values of the CL.

The second model improves on the NRL by generalizing the approach in Ref. (*25*) (GMS) to ion-ion collisions. Note that Eq. (7) tends to zero at low temperatures and does not include electron screening. This needs to be repaired for collision between screened strongly coupled ions. Choosing $b_{\max} = \lambda_{\text{eff}}$

$$\lambda_{\text{eff}} = \left[\frac{1}{\lambda_{\text{TF}}^2} + \sum_{\alpha=1}^{2} \frac{1}{\lambda_\alpha^2 + a_{\text{ws}}^2/x_\alpha} \right]^{-1/2}, \tag{9}$$

addresses this problem (*18*). The parameter λ_{TF} is the Thomas-Fermi length calculated from the electron temperature, T_e, and density, n_e, see Eq. (23) in Ref. (*18*). Note that Eq. (9) gives a positive definite value even at zero temperature. Finally, the GMS collision frequency appropriate for strongly-coupled plasmas is

$$\nu_{ij}^{\text{GMS}} = n_j \Phi \mathcal{S}^{\text{GMS}}, \tag{10}$$

$$\mathcal{S}^{\text{GMS}} = \frac{1}{2} \ln \left[1 + \left(\frac{2\lambda_{\text{eff}}}{b_{\min}} \right)^2 \right]. \tag{11}$$

The third model is presented in detail in Ref. (*53*) and it is based on a multispecies Bhatnagar-Gross-Krook solution of the Boltzmann equation. The main difference from the NRL and GMS models is that the collisional integral is calculated numerically using a Yukawa interaction, instead of a bare Coulomb interaction, and without any assumption of weak-scattering (*18*). This leads to a collisional frequency given by

$$\nu_{ij}^{\text{SMT}} = n_j \Phi \mathcal{S}^{\text{SMT}}, \tag{12}$$

$$\mathcal{S}^{\text{SMT}} = \frac{128}{3} \frac{\sqrt{\pi}}{2^{3/2}} \mathcal{K}_{11}(g), \tag{13}$$

where g is the thermally-averaged ion-ion Coulomb coupling factor,

$$g = \left(\frac{Z_1 Z_2 e^2}{4\pi\epsilon_0} \right) \frac{1}{k_B T_{\text{avg}}} \frac{1}{\lambda_{\text{eff}}}. \tag{14}$$

Typical values in our experiments are $g \sim 0.5$. The collision integral $\mathcal{K}_{11}(g)$ is calculated from Eqs. (C22-C24) in Appendix C of Ref. (*18*) with $n = m = 1$.

Experimental details

In the experiment, up to 20 million Ca and Yb atoms are trapped in a dual-species magneto-optical trap (MOT) (*11, 46*). The spatial density profile of the trapped neutral atoms is approximately spherically symmetric and Gaussian, $n = n_0 \exp[-r^2/(2\sigma^2)]$ with an rms size $\sigma \approx 300$ μm and peak density $n_0 \lesssim 4 \times 10^{10}$ cm^{-3}. The two MOTs are centered and spatially overlapped. The temperature of the atoms is around 0.002 K. We use resonant two stage photo-ionization to ionize 100% of Ca atoms and up to 60% of Yb atoms. The electron temperature is determined by the photon energy of the ionizing pulse above the ionization threshold, and a typical value is $T_e = 96$ K. The initial plasma densities are controlled by expanding the neutral atom cloud prior to ionization. The Ca and Yb atoms can expand for different lengths of time up to 2 ms, allowing independent control of the relative densities of these species. The process of loading the neutral atom trap, expanding the neutral atom clouds, and generating the plasma takes several ms and the process is repeated at a rate of 10 Hz.

The Ca^+ and Yb^+ velocity distributions are measured using laser-induced-fluorescence. Probe lasers at 393 (Ca^+) and 369 nm (Yb^+) overlapped using a dichroic mirror and then coupled into a single mode polarization maintaining optical fiber. The fiber output is collimated with a diameter of several mm and then cylindrically focused to illuminate a sheet of ions in the center of the plasma (*55*) (see Fig. 1. The laser intensities are typically 10 to 20% of the saturation intensity. For Ca^+, lasers at 854 and 850 nm prevent optical pumping into the metastable ^2D states. We verify that optical pumping is a negligible source of error.

Details of the measurement process are given in Fig. 1. With the probe laser frequencies at a particular offset from resonance, we collect fluorescence as a function of time after the plasma is created (*56*). Fluorescence measurements from up to 100 identical plasmas are averaged at a given frequency of the probe lasers. The probe laser frequency is changed and the measurement process is repeated. Using 11 different probe laser frequency offsets, we sample the ion velocity

distributions, using the Doppler shift to convert frequency offset to ion velocity. The data is post-processed so that at a given time after ionization, the fluorescence signal as a function of *frequency* is fit to a Voigt profile, and the rms Gaussian width, $v_{\alpha,\mathrm{th}}$, is used as a fit parameter. This is used to determine the ion temperature, T_α.

Two-temperature plasmas

The two-temperature nature of the plasma arises naturally because of the mass difference between the species. Although the ions initially retain the mK temperatures of the neutral atom cloud, the ion velocity distributions rapidly broaden as individual ions respond to the sudden appearance of neighboring ions (*57*). This disorder-induced heating (DIH) occurs because in the neutral atom cloud the atom pair distribution function is flat, $g(r) = 1$. As the ions push neighboring ions away, the pair distribution function develops a hole near $r = 0$ and the energy required to do that appears as increased kinetic energy of the ions, with temperatures near 1 K (*58*).

In a dual-species DIH process, the lower mass ions reach a higher temperature. The average kinetic energy of each species of ions in the plasma can be written as

$$k_B T_\alpha(t) = \frac{m_\alpha}{3N_\alpha} \sum_{i=1}^{N_\alpha} v_i^2(t), \tag{15}$$

where the index i indicates the particle of ion species α. We propagate the velocity in time using an Euler step, $v_i^2(t) = [\vec{v}_i(0) + \vec{a}_i(0)t]^2 = v_i^2(0) + 2\vec{v}_i(0) \cdot \vec{a}_i(0)t + a_i(0)^2 t^2$. In a uniform plasma with no spatial order and no bulk flow, the dot product $\vec{v}_i(0) \cdot \vec{a}_i(0)$ averages to zero and Eq. (15) simplifies to

$$\begin{aligned} k_B T_\alpha(t) &= \frac{m_\alpha}{3N_\alpha} \sum_{i=1}^{N_\alpha} \left[v_i^2(0) + a_i(0)^2 t^2 \right] \\ &= k_B T_\alpha(0) + \frac{t^2}{3N_\alpha m_\alpha} \sum_{i=1}^{N_\alpha} F_i^2(0), \end{aligned} \tag{16}$$

where we have used Newton's second law for the force magnitude F_i. This force is due to the electrostatic interaction and is mass independent. As Eq. (16) shows, the smaller mass will reach a higher temperature in the DIH process when the DIH timescale is faster than the thermal relaxation rate.

Molecular Dynamics Simulations

Experimental results are compared with MD simulations. These are carried out using the Sarkas package, a pure python open-source molecular dynamics code for non-ideal plasma simulation (*59*). Ion-ion interactions are represented using a Yukawa interaction,

$$U(r_{\alpha\beta}) = \frac{Z_\alpha Z_\beta e^2}{4\pi\epsilon_0}\frac{1}{r_{\alpha\beta}} e^{-r_{\alpha\beta}/\lambda_{\rm TF}}. \tag{17}$$

The initial positions of the ions are randomly distributed along the three axis of the simulation box. The initial velocities, however, are chosen from normal distribution with an initial width $v^{(0)}_{\alpha,\rm rms} = \sqrt{k_B T_0/m_\alpha}$ with $T_0 = 2$ mK.

Following the experiments, in the first 40 ns of the simulation Ca atoms are neutral, *i.e.* their charge number, Z, is set to 0, while Yb atoms carry a charge $Z = 1$. In this way only the Yb^+ atoms interact with each other and do not interact with Ca atoms. For $t \geq 40$ ns the charge number of Ca atoms is changed to 1 and the screening parameter $\kappa = a_{\rm ws}/\lambda_{\rm TF}$ is updated. Note that κ increases after the first 40 ns due to the increased electron density.

The potential energy and forces are calculated using a highly efficient Particle-Particle Particle-Mesh algorithm (*60*). This algorithm is more reliable than the minimum image convention when κ is small. Electron temperature and densities from the experiments lead to $\kappa \sim 0.37 - 0.46$.

MD simulations are performed for plasmas with a uniform spatial density, obtained from experimental values, and periodic boundary conditions. While the experiments necessarily have open boundary conditions, the MD simulations are an appropriate representations of the middle

of the plasma when the thermalization time is faster than the expansion time. For these initial conditions there is no equilibration phase. Particle positions and velocities are integrated using the standard velocity Verlet algorithm. The timestep and total number of particles were varied and chosen to give converged results. In our simulations, we use $N = 50,000$ total ions, with Ca/Yb number ratios matching those of the experiments. The timesteps were chosen such that $\omega_p \Delta t \sim 0.002$. For each experiment five MD Non-equilibrium simulations with different initial conditions were performed.

Because UNPs are created out of equilibrium (*57*), we need to verify when a two-temperature system has formed, *i.e.* when the velocity distribution of each species has relaxed to a Maxwellian distribution. We use an analysis based on the Hermite expansion of velocity distribution to quantify the deviations from a Maxwellian distribution, $\mathcal{M}(v)$, (*61, 62*). The expansion reads as

$$f(v,t) = \mathcal{M}(v) \sum_{n=0} \frac{1}{n!} a_n(t) \mathcal{H}_n(v), \tag{18}$$

where $\mathcal{H}_n(v)$ are the probabilistic Hermite polynomials of order n.

In the case of a Maxwellian distribution the Hermite coefficients, a_n will all vanish except for $a_0 = 1$. The even and odd coefficients of the expansion, a_n, are related to the even and odd moments of the velocity distribution respectively. In Fig. 2 the top panels show time evolution plots of the $|a_2/2|$ (a) and $a_4/4!$ (b) coefficients of the Hermite expansion. The bottom panels quantify the deviations from a Maxwellian distribution; (c) percentage deviations of the Maxwellian rms width obtained from Eq. (18) and MD rms velocity, (d) percentage of the number of Maxwellian particles. We find that after ~ 1 μs the two temperature system is well established. The number of ions that lie outside of a Maxwellian distribution can be calculated by fitting the MD velocity distribution to a normalized Gaussian and then integrating the absolute value of the difference. In this way it can be shown that a Maxwellian distribution is appropriate for 90% of all the particles by $t = 0.5$ μs. By $t = 1.0$ μs, the fraction is 98%, see

panel d) of Fig. 2.

Results and Discussion

In Fig. 3 we plot the Ca^+ and Yb^+ ion temperatures and temperature differences. To enforce compatibility in comparing the MD data to the experiment, the MD velocity distribution is convolved with a Lorentzian distribution and then fit to a Voigt profile with the Gaussian width as a fit parameter. This slightly underestimates the average ion kinetic energy during the DIH phase (*55*) because of slight departures from a Maxwellian velocity distribution (see Fig. 2).

For lower density plasmas in Fig. 3a, the laboratory temperature measurements and MD simulations agree well. For the higher density plasmas in Fig. 3b, the temperatures exhibit a systematic departure. However, the temperature difference plotted in Fig. 3d shows excellent agreement between the laboratory measurements and the MD. Experimentally, higher densities correspond to smaller plasmas with smaller initial size and larger density gradients. The absolute value of the Temperature measurements in these smaller plasmas may depend somewhat on the cylindrical focus of the probe laser beam into the plasma.

In Fig. 4 we compare MD results with the theoretical predictions presented above. The progression of models begins with standard plasma theory that incorporates physically motivated ion trajectories, Eqs. (4)-(8) (*25*). This is plotted as dotted blue line and it indicates a serious deficiency of standard plasma theory. This is expected since this model, Eq. (6), uses the ion Debye length as the relevant length scale. The next level of improvement provides a correction for strong coupling when the Debye length becomes unphysically small, Eqs. (10)-(11). This is plotted as dash-dot orange line. This strong coupling correction brings the theory closer to the simulations, but still underpredicts the relaxation rates.

Our best model is based on an effective potential in a Boltzmann description, Eqs. (12)-(14), which includes velocity dependent strong scattering. This is plotted as a dashed green line in

Fig. 4. This incorporates strong scattering in a self consistent way, reducing the ambiguity in choosing *ad hoc* cut off parameters inherent in a Coulomb logarithm approach. Nonetheless this model predicts temperature relaxation rates somewhat faster than the MD result. This is surprising given the previously demonstrated accuracy of this model in reproducing experimental data and MD simulations of momentum transfer, joule heating, diffusion, viscosity, thermal conductivity, etc. (*11, 18, 46*).

This overprediction may be due to errors in the effective potential, non-binary collisions, or coupled modes (*26, 27, 63, 64*). The influence of the coupled mode can be identified when examining the dielectric response function $\varepsilon(\mathbf{k},\omega)$ of a binary plasma mixture. In a Lenard-Balescu approach the $\varepsilon(\mathbf{k},\omega)$ dependence of the temperature relaxation rate is (*65*),

$$\begin{aligned}\nu_{12} \quad \propto \quad & \sum_{\mathbf{k}} \int d\omega \frac{(\phi_{12})^2}{|\varepsilon(\mathbf{k},\omega)|^2} \left\{ \frac{T_1}{n_1} \left[\operatorname{Im} \chi_1^0\right]^2 \left|1-\phi_{22}\chi_2^0\right|^2 \right. \\ & \left. -\frac{T_2}{n_2} \left[\operatorname{Im} \chi_2^0\right]^2 \left|1-\phi_{11}\chi_1^0\right|^2 \right\} \end{aligned} \tag{19}$$

where $\chi_\alpha^0(\mathbf{k},\omega)$ is the ideal gas response function of each species, $\phi_{\alpha\beta}(k)$ is the Fourier transform of the Coulomb interaction between the two ion species. In the low frequency (static) limit the effective interaction $\phi_{12}(k)/\varepsilon(\mathbf{k},\omega)$ gives the Yukawa-like interaction of Eq. (17). The three models described above neglect the frequency dependence of $\varepsilon(\mathbf{k},\omega)$ and consider only the static version $\phi_{12}(k)/\varepsilon(\mathbf{k},0)$. This effective interaction is then used to inform the Coulomb logarithm in a Fokker-Planck approach (NRL, GMS) or the cross section in a Boltzmann equation (SMT).

In general the effective interaction is time and frequency dependent. The electron-ion and ion-ion dynamics need to be considered when extending SMT to include coupled modes. Some of these processes harden the ion-ion potential while others soften it. Future work is needed in this direction.

In conclusion, we demonstrate that UNPs provide an new platform for studying ion trans-

port properties in a two-temperature system. We characterized the approach to equilibrium using a Hermite expansion, which reveals when a relaxing system can be safely treated as a "two-temperature" system. This powerful approach facilitates comparison of data with quasi-equilibrium theories.

We present the first measurement of ion-ion temperature relaxation rates in a newly developed strongly coupled binary ionic mixture. Using a single diagnostic method we directly measure the ion temperatures without inference through, for example, an equation of state. This shows the remarkable capability for UNPs to investigate component physics across coupling regimes, simulating some aspects of, *e.g.* HEDP, plasma mixtures, and liquid metal alloys.

We show that our MD simulations of temperature relaxation agree with experimental measurements. This reinforces the fact that the Yukawa potential, Eq. (17), accurately describes ion-ion interaction in dual-species UNP mixtures. This further confirms the ability of our MD simulations to capture a very complex relaxation process. This confidence, in turn, allows us to employ the MD as a surrogate for information that the experiment cannot provide, as as the Hermite coefficients. These observations reinforce the importance of having MD as a an integral part of experimental workflows.

We compare the simulated relaxation rates with three popular temperature relaxation theories of varying fidelity. The closest theory is based on solving the Boltzmann equation using an effective potential. The variance between this theory and the MD simulations is likely caused by coupled modes, an effect that is omitted from the theory by design. Future work could explore the influence of coupled modes on ion transport. Incorporating coupled modes into the Boltzmann solutions could also prove fruitful for ion transport in the regime of relatively small mass ratios.

References and Notes

1. O. A. Hurricane, D. A. Callahan, D. T. Casey, P. M. Celliers, C. Cerjan, E. L. Dewald, T. R. Dittrich, T. Döppner, D. E. Hinkel, L. F. B. Hopkins, J. L. Kline, S. L. Pape, T. Ma, A. G. MacPhee, J. L. Milovich, A. Pak, H.-S. Park, P. K. Patel, B. A. Remington, J. D. Salmonson, P. T. Springer, R. Tommasini, Fuel gain exceeding unity in an inertially confined fusion implosion. *Nature* **506**, 343–348 (2014).

2. R. Tommasini, J. E. Field, B. A. Hammel, O. L. Landen, S. W. Haan, C. Aracne-Ruddle, L. R. Benedetti, D. K. Bradley, D. A. Callahan, E. L. Dewald, T. Doeppner, M. J. Edwards, O. A. Hurricane, N. Izumi, O. A. Jones, T. Ma, N. B. Meezan, S. R. Nagel, J. R. Rygg, K. S. Segraves, M. Stadermann, R. J. Strauser, R. P. J. Town, Tent-induced perturbations on areal density of implosions at the national ignition facilitya). *Physics of Plasmas* **22**, 056315 (2015).

3. L. B. Fletcher, A. L. Kritcher, A. Pak, T. Ma, T. Döppner, C. Fortmann, L. Divol, O. S. Jones, O. L. Landen, H. A. Scott, J. Vorberger, D. A. Chapman, D. O. Gericke, B. A. Mattern, G. T. Seidler, G. Gregori, R. W. Falcone, S. H. Glenzer, Observations of continuum depression in warm dense matter with x-ray thomson scattering. *Phys. Rev. Lett.* **112**, 145004 (2014).

4. Y. Zhou, Rayleigh–taylor and richtmyer–meshkov instability induced flow, turbulence, and mixing. II. *Physics Reports* **723-725**, 1–160 (2017).

5. Y. Zhou, T. T. Clark, D. S. Clark, S. G. Glendinning, M. A. Skinner, C. M. Huntington, O. A. Hurricane, A. M. Dimits, B. A. Remington, Turbulent mixing and transition criteria of flows induced by hydrodynamic instabilities. *Physics of Plasmas* **26**, 080901 (2019).

6. J. Clérouin, P. Arnault, B.-J. Gréa, S. Guisset, M. Vandenboomgaerde, A. J. White, L. A. Collins, J. D. Kress, C. Ticknor, Static and dynamic properties of multi-ionic plasma mixtures. *Phys. Rev. E* **101**, 033207 (2020).

7. J. B. Taylor, Plasma diffusion in two dimensions. *Physics of Fluids* **14**, 1492 (1971).

8. P. Arnold, G. D. Moore, L. G. Yaffe, Transport coefficients in high temperature gauge theories (i): leading-log results. *Journal of High Energy Physics* **2000**, 001–001 (2000).

9. Z. Donkó, P. Hartmann, Shear viscosity of strongly coupled yukawa liquids. *Phys. Rev. E* **78**, 026408 (2008).

10. C. Ticknor, J. D. Kress, L. A. Collins, J. Clérouin, P. Arnault, A. Decoster, Transport properties of an asymmetric mixture in the dense plasma regime. *Phys. Rev. E* **93**, 063208 (2016).

11. S. D. Bergeson, S. D. Baalrud, C. L. Ellison, E. Grant, F. R. Graziani, T. C. Killian, M. S. Murillo, J. L. Roberts, L. G. Stanton, Exploring the crossover between high-energy-density plasma and ultracold neutral plasma physics. *Physics of Plasmas* **26**, 100501 (2019).

12. M. S. Murillo, M. W. C. Dharma-wardana, Temperature relaxation in hot dense hydrogen. *Phys. Rev. Lett.* **100**, 205005 (2008).

13. Q. Ma, J. Dai, D. Kang, M. S. Murillo, Y. Hou, Z. Zhao, J. Yuan, Extremely low electron-ion temperature relaxation rates in warm dense hydrogen: Interplay between quantum electrons and coupled ions. *Phys. Rev. Lett.* **122**, 015001 (2019).

14. Q. Ma, J. Dai, D. Kang, M. S. Murillo, Y. Hou, Z. Zhao, J. Yuan, Erratum: Extremely low electron-ion temperature relaxation rates in warm dense hydrogen: Interplay between

quantum electrons and coupled ions [phys. rev. lett. 122, 015001 (2019)]. *Phys. Rev. Lett.* **123**, 099901 (2019).

15. A. Ng, Outstanding questions in electron–ion energy relaxation, lattice stability, and dielectric function of warm dense matter. *International Journal of Quantum Chemistry* **112**, 150-160 (2012).

16. B. Paxton, J. Schwab, E. B. Bauer, L. Bildsten, S. Blinnikov, P. Duffell, R. Farmer, J. A. Goldberg, P. Marchant, E. Sorokina, A. Thoul, R. H. D. Townsend, F. X. Timmes, Modules for experiments in stellar astrophysics (${\mathtt{m}}{\mathtt{e}}{\mathtt{s}}{\mathtt{a}}$): Convective boundaries, element diffusion, and massive star explosions. *The Astrophysical Journal Supplement Series* **234**, 34 (2018).

17. R. A. Heinonen, D. Saumon, J. Daligault, C. E. Starrett, S. D. Baalrud, G. Fontaine, Diffusion coefficients in the envelopes of white dwarfs. *The Astrophysical Journal* **896**, 2 (2020).

18. L. G. Stanton, M. S. Murillo, Ionic transport in high-energy-density matter. *Phys. Rev. E* **93**, 043203 (2016).

19. L. X. Benedict, M. P. Surh, J. I. Castor, S. A. Khairallah, H. D. Whitley, D. F. Richards, J. N. Glosli, M. S. Murillo, C. R. Scullard, P. E. Grabowski, *et al.*, Molecular dynamics simulations and generalized lenard-balescu calculations of electron-ion temperature equilibration in plasmas. *Physical Review E* **86**, 046406 (2012).

20. L. X. Benedict, J. N. Glosli, D. F. Richards, F. H. Streitz, S. P. Hau-Riege, R. A. London, F. R. Graziani, M. S. Murillo, J. F. Benage, Molecular dynamics simulations of electron-ion temperature equilibration in an s f 6 plasma. *Physical review letters* **102**, 205004 (2009).

21. H. A. Gould, H. E. DeWitt, Convergent kinetic equation for a classical plasma. *Phys. Rev.* **155**, 68–74 (1967).

22. P. E. Grabowski, M. P. Surh, D. F. Richards, F. R. Graziani, M. S. Murillo, Molecular dynamics simulations of classical stopping power. *Phys. Rev. Lett.* **111**, 215002 (2013).

23. S. D. Baalrud, J. Daligault, Mean force kinetic theory: A convergent kinetic theory for weakly and strongly coupled plasmas. *Physics of Plasmas* **26**, 082106 (2019).

24. M. S. Murillo, J. Weisheit, S. B. Hansen, M. W. C. Dharma-wardana, Partial ionization in dense plasmas: Comparisons among average-atom density functional models. *Phys. Rev. E* **87**, 063113 (2013).

25. D. Gericke, M. Murillo, M. Schlanges, Dense plasma temperature equilibration in the binary collision approximation. *Physical Review E* **65**, 036418 (2002).

26. M. W. C. Dharma-wardana, F. m. c. Perrot, Energy relaxation and the quasiequation of state of a dense two-temperature nonequilibrium plasma. *Phys. Rev. E* **58**, 3705–3718 (1998).

27. M. W. C. Dharma-wardana, F. m. c. Perrot, Erratum: Energy relaxation and the quasiequation of state of a dense two-temperature nonequilibrium plasma [phys. rev. e 58, 3705 (1998)]. *Phys. Rev. E* **63**, 069901 (2001).

28. G. Hazak, Z. Zinamon, Y. Rosenfeld, M. W. C. Dharma-wardana, Temperature relaxation in two-temperature states of dense electron-ion systems. *Phys. Rev. E* **64**, 066411 (2001).

29. M. Dharma-wardana, Hot-electron relaxation in dense 'two-temperature' hydrogen. *arXiv:1705.10221* (2017).

30. B. I. Cho, T. Ogitsu, K. Engelhorn, A. A. Correa, Y. Ping, J. W. Lee, L. J. Bae, D. Prendergast, R. W. Falcone, P. A. Heimann, Measurement of electron-ion relaxation in warm dense copper. *Scientific Reports* **6** (2016).

31. J. Daligault, J. Simoni, Theory of the electron-ion temperature relaxation rate spanning the hot solid metals and plasma phases. *Phys. Rev. E* **100**, 043201 (2019).

32. J. Simoni, J. Daligault, First-principles determination of electron-ion couplings in the warm dense matter regime. *Phys. Rev. Lett.* **122**, 205001 (2019).

33. J. Vorberger, D. O. Gericke, T. Bornath, M. Schlanges, Energy relaxation in dense, strongly coupled two-temperature plasmas. *Phys. Rev. E* **81**, 046404 (2010).

34. A. J. Kemp, Y. Sentoku, V. Sotnikov, S. C. Wilks, Collisional relaxation of superthermal electrons generated by relativistic laser pulses in dense plasma. *Phys. Rev. Lett.* **97**, 235001 (2006).

35. G. Hazak, Z. Zinamon, Y. Rosenfeld, M. W. C. Dharma-wardana, Temperature relaxation in two-temperature states of dense electron-ion systems. *Phys. Rev. E* **64**, 066411 (2001).

36. F. R. Graziani, V. S. Batista, L. X. Benedict, J. I. Castor, H. Chen, S. N. Chen, C. A. Fichtl, J. N. Glosli, P. E. Grabowski, A. T. Graf, *et al.*, Large-scale molecular dynamics simulations of dense plasmas: The cimarron project. *High Energy Density Physics* **8**, 105–131 (2012).

37. J. Vorberger, D. Gericke, Comparison of electron–ion energy transfer in dense plasmas obtained from numerical simulations and quantum kinetic theory. *High Energy Density Physics* **10**, 1–8 (2014).

38. G. Dimonte, J. Daligault, Molecular-dynamics simulations of electron-ion temperature relaxation in a classical coulomb plasma. *Phys. Rev. Lett.* **101**, 135001 (2008).

39. J. Glosli, F. Graziani, R. More, M. Murillo, F. Streitz, M. Surh, L. Benedict, S. Hau-Riege, A. Langdon, R. London, Molecular dynamics simulations of temperature equilibration in dense hydrogen. *Physical Review E* **78**, 025401 (2008).

40. C. S. Jones, M. S. Murillo, Analysis of semi-classical potentials for molecular dynamics and monte carlo simulations of warm dense matter. *High Energy Density Physics* **3**, 379–394 (2007).

41. P. E. Grabowski, A. Markmann, I. V. Morozov, I. A. Valuev, C. A. Fichtl, D. F. Richards, V. S. Batista, F. R. Graziani, M. S. Murillo, Wave packet spreading and localization in electron-nuclear scattering. *Phys. Rev. E* **87**, 063104 (2013).

42. G. Dharuman, J. Verboncoeur, A. Christlieb, M. S. Murillo, Atomic bound state and scattering properties of effective momentum-dependent potentials. *Phys. Rev. E* **94**, 043205 (2016).

43. P. McQuillen, T. Strickler, T. Langin, T. C. Killian, Ion temperature evolution in an ultracold neutral plasma. *Physics of Plasmas* **22**, 033513 (2015).

44. G. Bannasch, J. Castro, P. McQuillen, T. Pohl, T. C. Killian, Velocity relaxation in a strongly coupled plasma. *Phys. Rev. Lett.* **109**, 185008 (2012).

45. T. S. Strickler, T. K. Langin, P. McQuillen, J. Daligault, T. C. Killian, Experimental measurement of self-diffusion in a strongly coupled plasma. *Phys. Rev. X* **6**, 021021 (2016).

46. T. Sprenkle, A. Dodson, Q. McKnight, R. Spencer, S. Bergeson, A. Diaw, M. S. Murillo, Ion friction at small values of the coulomb logarithm. *Phys. Rev. E* **99**, 053206 (2019).

47. W.-T. Chen, C. Witte, J. L. Roberts, Observation of a strong-coupling effect on electron-ion collisions in ultracold plasmas. *Phys. Rev. E* **96**, 013203 (2017).

48. P. Jiang, J. L. Roberts, Electric field influences on the initial electron temperature of ultracold plasmas. *Physics of Plasmas* **26**, 043513 (2019).

49. M. Aghigh, K. Grant, R. Haenel, K. L. Marroquín, F. B. V. Martins, H. Sadegi, M. Schulz-Weiling, J. Sous, R. Wang, J. S. Keller, E. R. Grant, Dissipative dynamics of atomic and molecular rydberg gases: Avalanche to ultracold plasma states of strong coupling. *Journal of Physics B: Atomic, Molecular and Optical Physics* **53**, 074003 (2020).

50. J. Sous, E. Grant, Possible many-body localization in a long-lived finite-temperature ultracold quasineutral molecular plasma. *Phys. Rev. Lett.* **120**, 110601 (2018).

51. A. Ng, P. Celliers, G. Xu, A. Forsman, Electron-ion equilibration in a strongly coupled plasma. *Phys. Rev. E* **52**, 4299–4310 (1995).

52. L. G. Stanton, M. S. Murillo, Ionic transport in high-energy-density matter. *Phys. Rev. E* **93**, 043203 (2016).

53. J. R. Haack, C. D. Hauck, M. S. Murillo, A conservative, entropic multispecies bgk model. *Journal of Statistical Physics* **168**, 826–856 (2017).

54. J. D. Huba, *NRL PLASMA FORMULARY Supported by The Office of Naval Research* (Naval Research Laboratory, Washington, DC, 2013).

55. T. K. Langin, T. Strickler, N. Maksimovic, P. McQuillen, T. Pohl, D. Vrinceanu, T. C. Killian, Demonstrating universal scaling for dynamics of yukawa one-component plasmas after an interaction quench. *Phys. Rev. E* **93**, 023201 (2016).

56. Ion fluorescence is collected using an $f/2$ 1:4 optical relay imaging system to minimize the influence of the point-spread function inherent in the intensified camera.

57. Y. C. Chen, C. E. Simien, S. Laha, P. Gupta, Y. N. Martinez, P. G. Mickelson, S. B. Nagel, T. C. Killian, Electron screening and kinetic-energy oscillations in a strongly coupled plasma. *Phys. Rev. Lett.* **93**, 265003 (2004).

58. M. S. Murillo, Ultrafast dynamics of strongly coupled plasmas. *Phys. Rev. Lett.* **96**, 165001 (2006).

59. (accessed October 2020). https://murillo-group.github.io/sarkas/.

60. G. Dharuman, L. G. Stanton, J. N. Glosli, M. S. Murillo, A generalized ewald decomposition for screened coulomb interactions. *The Journal of Chemical Physics* **146**, 024112 (2017).

61. R. L. Liboff, *Kinetic theory: classical, quantum, and relativistic descriptions* (Springer Science & Business Media, 2003).

62. H. Grad, On the kinetic theory of rarefied gases. *Communications on Pure and Applied Mathematics* **2**, 331-407 (1949).

63. D. A. Chapman, J. Vorberger, D. O. Gericke, Reduced coupled-mode approach to electron-ion energy relaxation. *Phys. Rev. E* **88**, 013102 (2013).

64. P. Mabey, S. Richardson, T. G. White, L. B. Fletcher, S. H. Glenzer, N. J. Hartley, J. Vorberger, D. O. Gericke, G. Gregori, A strong diffusive ion mode in dense ionized matter predicted by langevin dynamics. *Nature Communications* **8** (2017).

65. S. Ichimaru, *Statistical Plasma Physics* (CRC Press, Boca Raton, Florida, 2004).

Acknowledgements

We thank Dr. Jeffrey Haack of Los Alamos National Laboratory for useful conversations. M.S.M. and L.G.S. were supported by the U.S. Air Force Office of Scientific Research Grant No. FA9550-17-1-0394. R.S.T. and S.D.B. acknowledge support from the U.S. Air Force Office of Scientific Research Grant No. FA9550-17-1-0302 and the National Science Foundation Grant No. PHY-2009999.

Author Information

The authors contributed equally to this work.

Contributions

R.S.T. and S.D.B. Conceived and built the experiment, designed and carried out the laboratory measurements, and performed the experimental data reduction. L.G.S. and M.S.M. Designed and performed the computer simulations and theoretical analysis and calculations. All authors contributed equally to the writing of the manuscript. All authors commented on the manuscript and agreed on its contents.

Corresponding authors

Correspondence to Scott Bergeson (scott.bergeson@byu.edu) and
Michael Murillo (murillom@msu.edu).

Ethics declarations

Competing interests

The authors declare no competing financial interests.

Data Availability

The data that support the findings of this study are available from the corresponding suthors upon reasonable request.

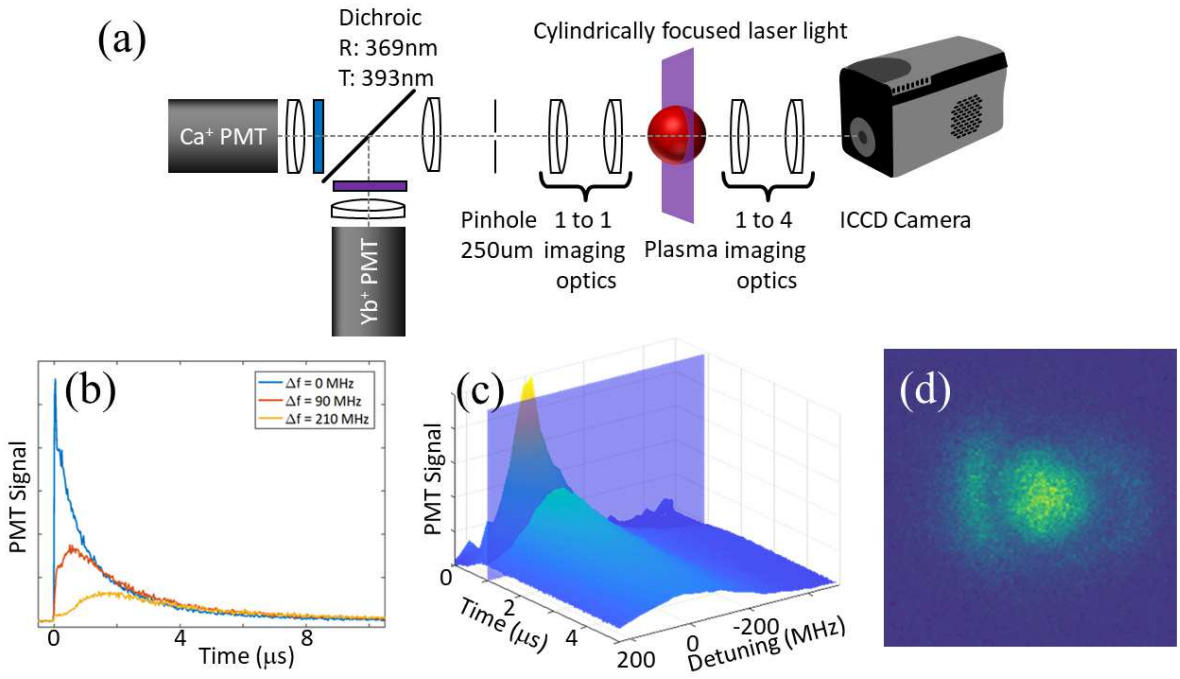

Figure 1: Experimental details for fluorescence detection from Ca^+ and Yb^+ ions. (a). Schematic diagram of the optical system used for fluorescence detection. The plasma is illuminated by cylindrically focused laser light. Laser-induced fluorescence is collected using an $f/2$ 1:1 imaging system. For PMT measurements the plasma is imaged onto a $\phi = 250$ μm aperture, enabling measurements of the central portion of the plasma. Spectral filters in front of the PMTs allow simultaneous measurements of fluorescence from both Ca^+ and Yb^+ ions. (b) Typical laser-induced fluorescence PMT signals. (c) A representation of laser-induced fluorescence measurements vs. time as a function of probe laser frequency detuning. (d) Typical Ca^+ fluorescence ICCD camera image when Yb^+ ions are present after a time-evolution of 2.5 μs. Camera measurements give spatial information at a particular time after ionization.

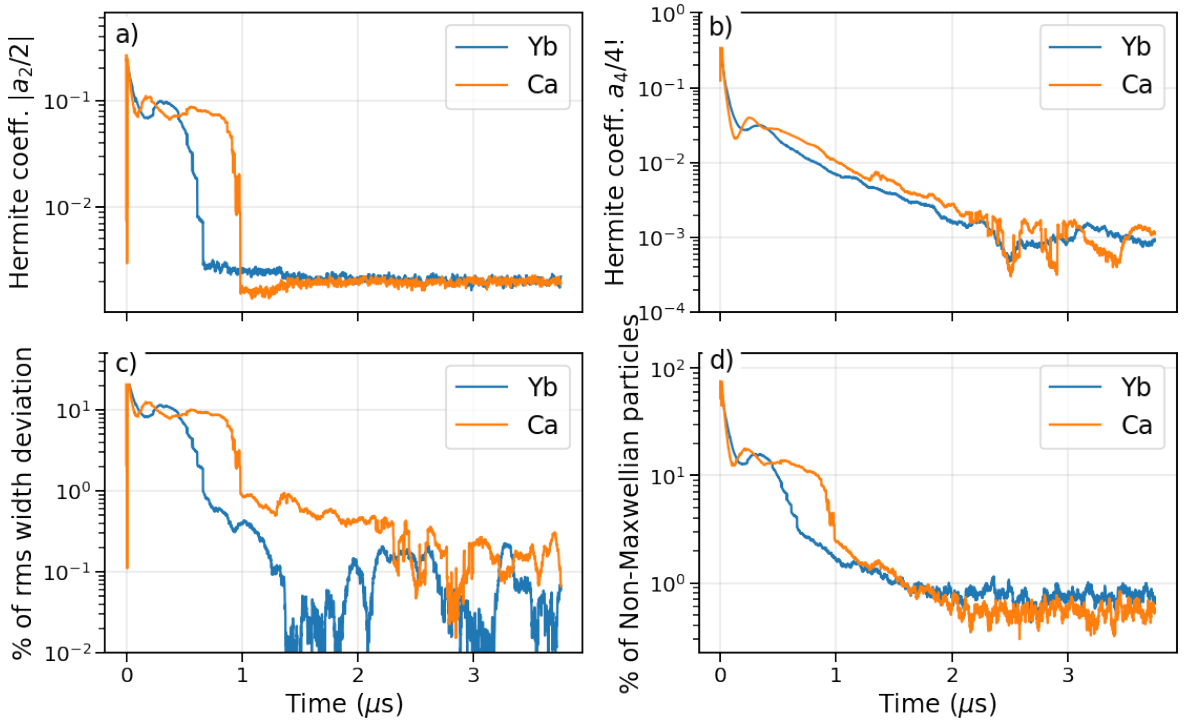

Figure 2: Time evolution of a) $a_2/2$ Hermite coefficient, b) $a_4/4!$ Hermite coefficient, c) percentage deviations of the Maxwellian rms width obtained from Eq. (18) and MD rms velocity, d) percentage of the number of Maxwellian particles. Simulation parameters $n_0^{Yb} = 1.9 \times 10^9$ cm^{-3}, $n_0^{Ca} = 3.4 \times 10^9$ cm^{-3}, $T_e = 100$ K, $\kappa = 0.38$.

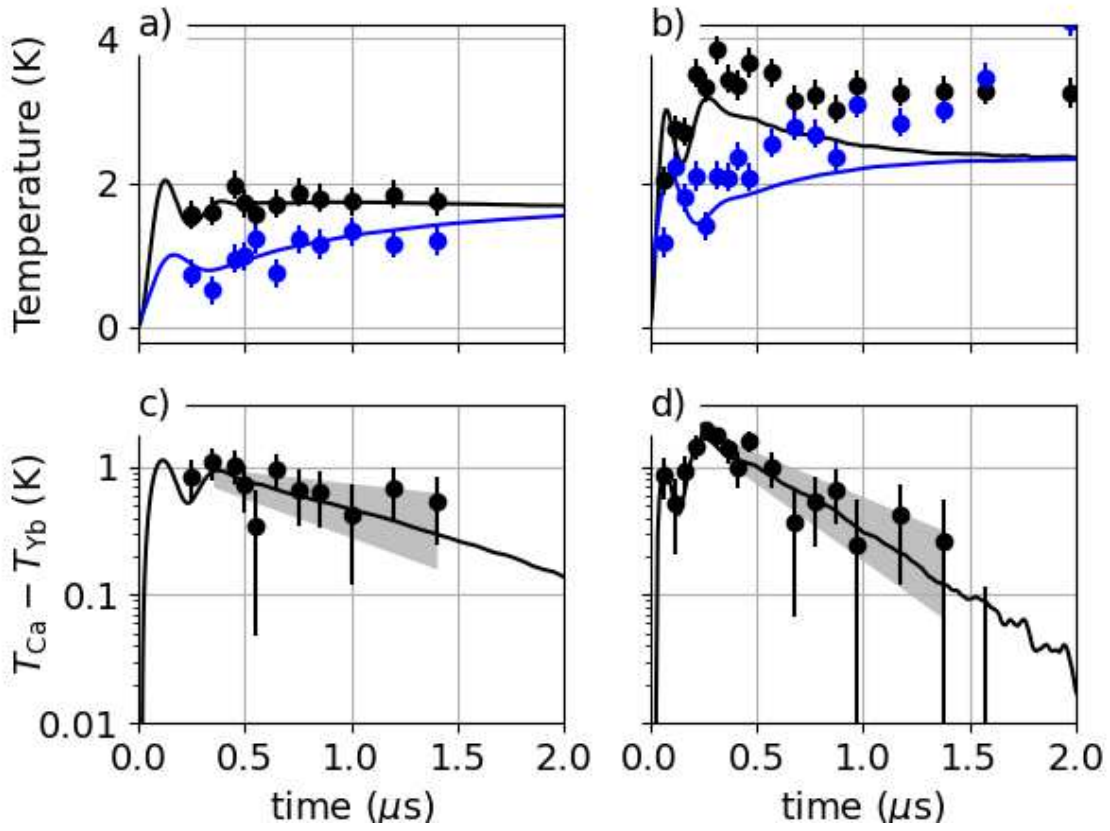

Figure 3: Temperature vs. time for two UNP configurations. a) T_{Ca} (black), $n_0^{\mathrm{Ca}} = 3.4 \times 10^9$ cm^{-3}, $\sigma_0^{\mathrm{Ca}} = 0.57$ mm, and T_{Yb} (blue), $n_0^{\mathrm{Yb}} = 1.9 \times 10^9$ cm^{-3}, $\sigma_0^{\mathrm{Yb}} = 0.72$ mm. Circles show temperatures extracted from laboratory data. Solid lines show MD data. c) Temperature difference, T_{Ca} - T_{Yb}. Circles show laboratory data. Solid lines show MD data. The gray shaded area represents the estimated 1-σ uncertainties in the decay rate extracted from the laboratory data. Panels b) and d) show the same analysis for a higher density plasma with $n_0^{\mathrm{Ca}} = 4.3 \times 10^9$ cm^{-3}, $\sigma_0^{\mathrm{Ca}} = 0.53$ mm, and $n_0^{\mathrm{Yb}} = 1.3 \times 10^{10}$ cm^{-3}, $\sigma_0^{\mathrm{Yb}} = 0.38$ mm. For all of this data, the electron temperature is 96 K.

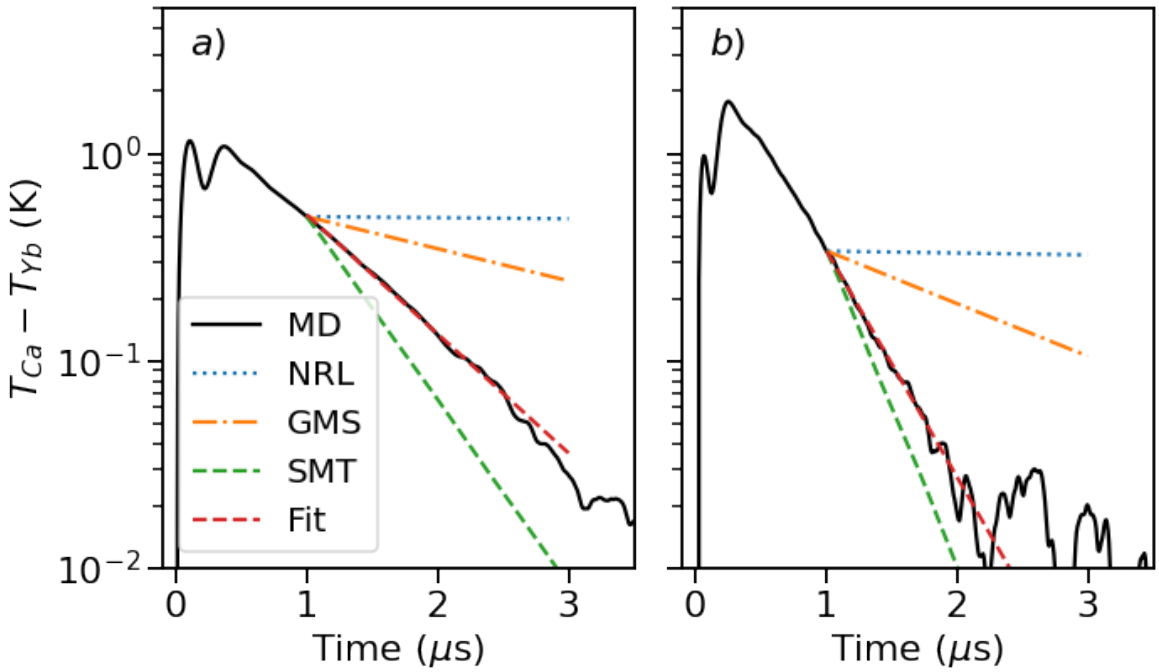

Figure 4: Semilog plot of the temperature difference $T_{\mathrm{Ca}} - T_{\mathrm{Yb}}$ compared with temperature relaxation models. NRL dotted blue line, Eqs. (4 - 8), GMS dash-dot orange line, Eqs. (10)-(11), SMT dashed green line, Eqs. (12-13), and exponential fit for the same systems as in Fig. 3 Simulation parameters $T_e = 100$ K, a) $\kappa = 0.38$, $n_0^{Yb} = 1.9 \times 10^9$ cm^{-3}, $n_0^{Ca} = 3.4 \times 10^9$ cm^{-3}, exponential fit parameter $\nu = 1.30 \times 10^6$ Hz b) $\kappa = 0.46$, $n_0^{Yb} = 1.3 \times 10^{10}$ cm^{-3}, $n_0^{Ca} = 4.3 \times 10^9$ cm^{-3} exponential fit parameter $\nu = 2.52 \times 10^6$ Hz

Figures

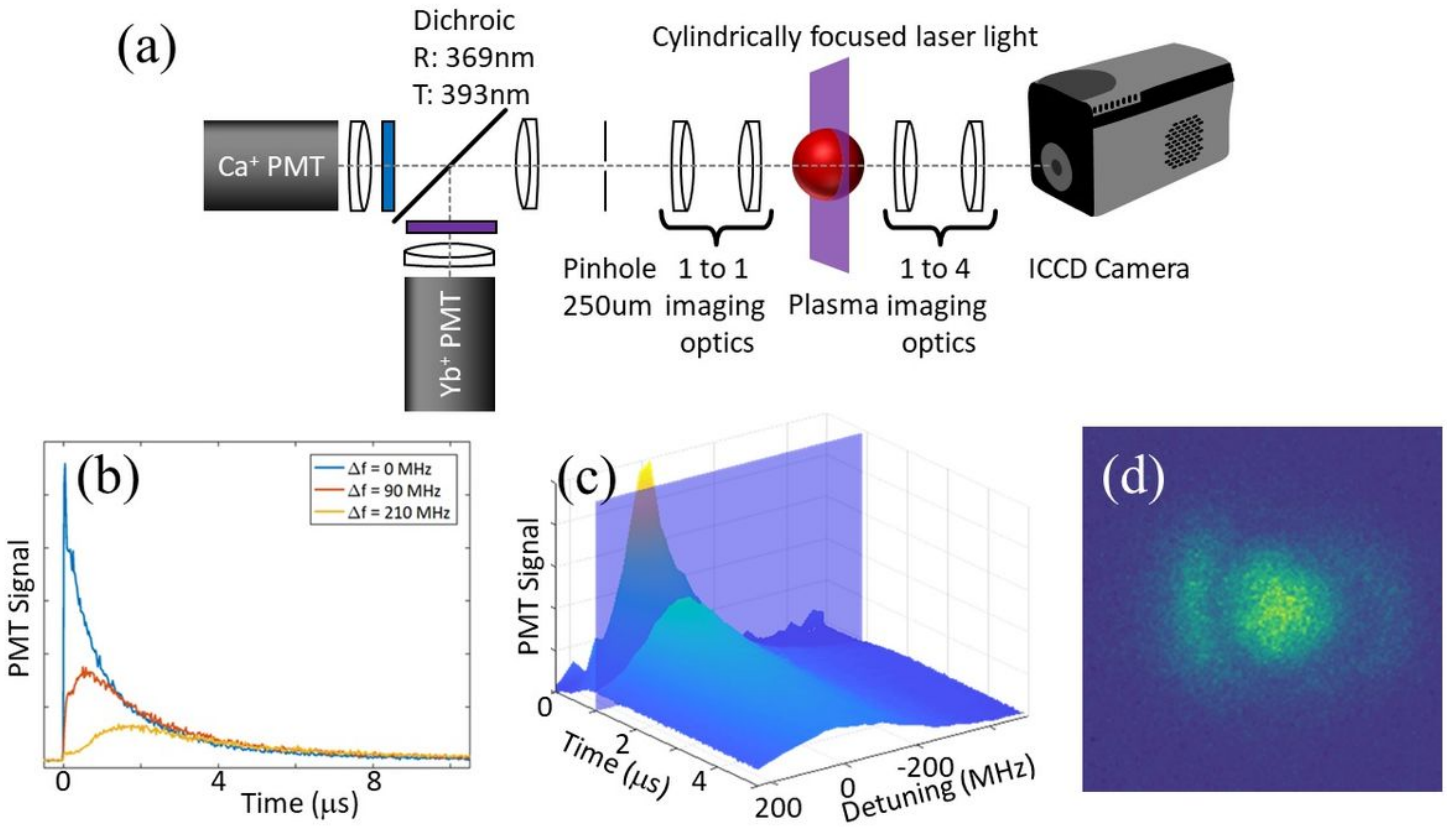

Figure 1

Experimental details for fluorescence detection from Ca+ and Yb+ ions. (See Manuscript file for full figure caption)

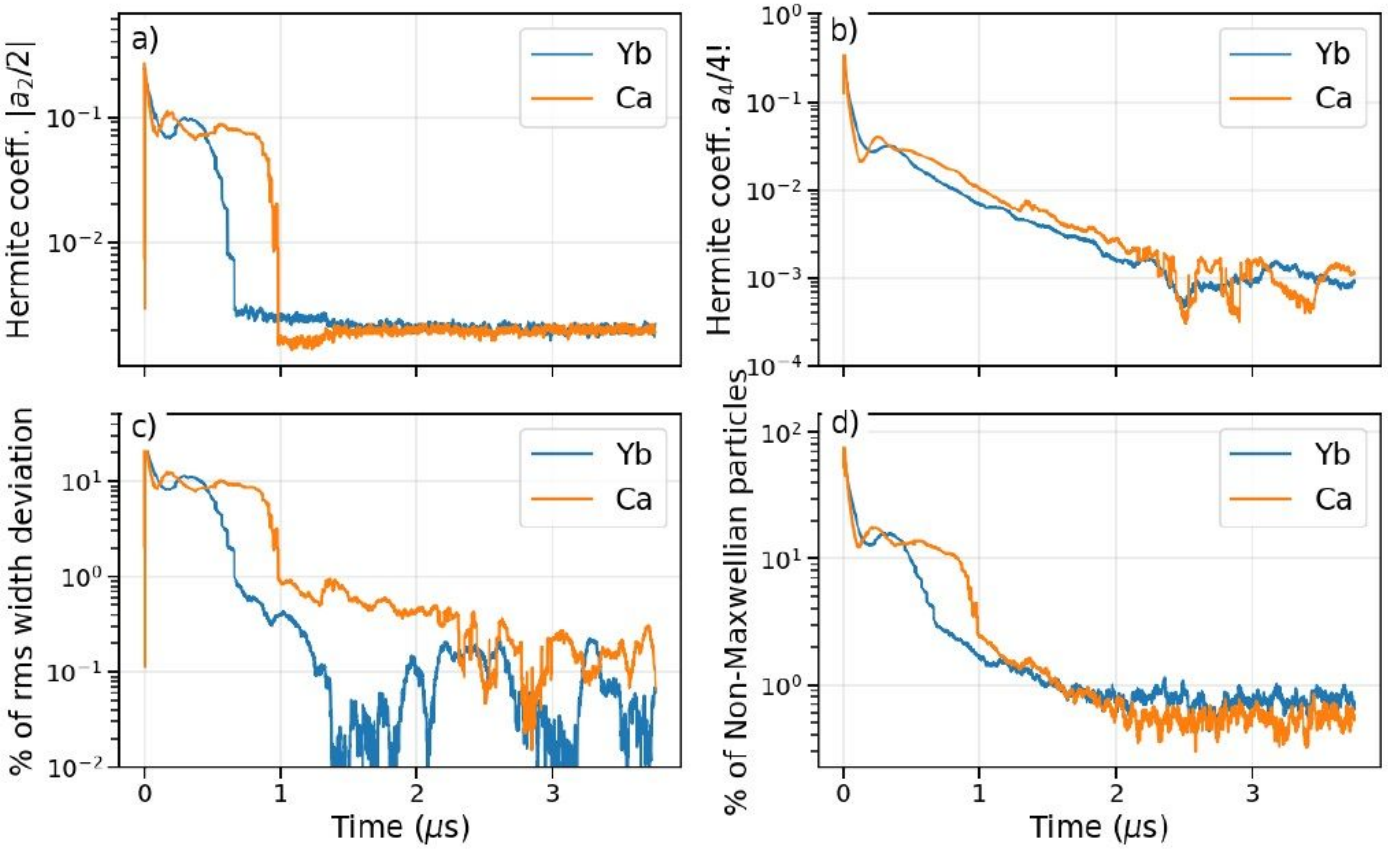

Figure 2

Time evolution (See Manuscript file for full figure caption)

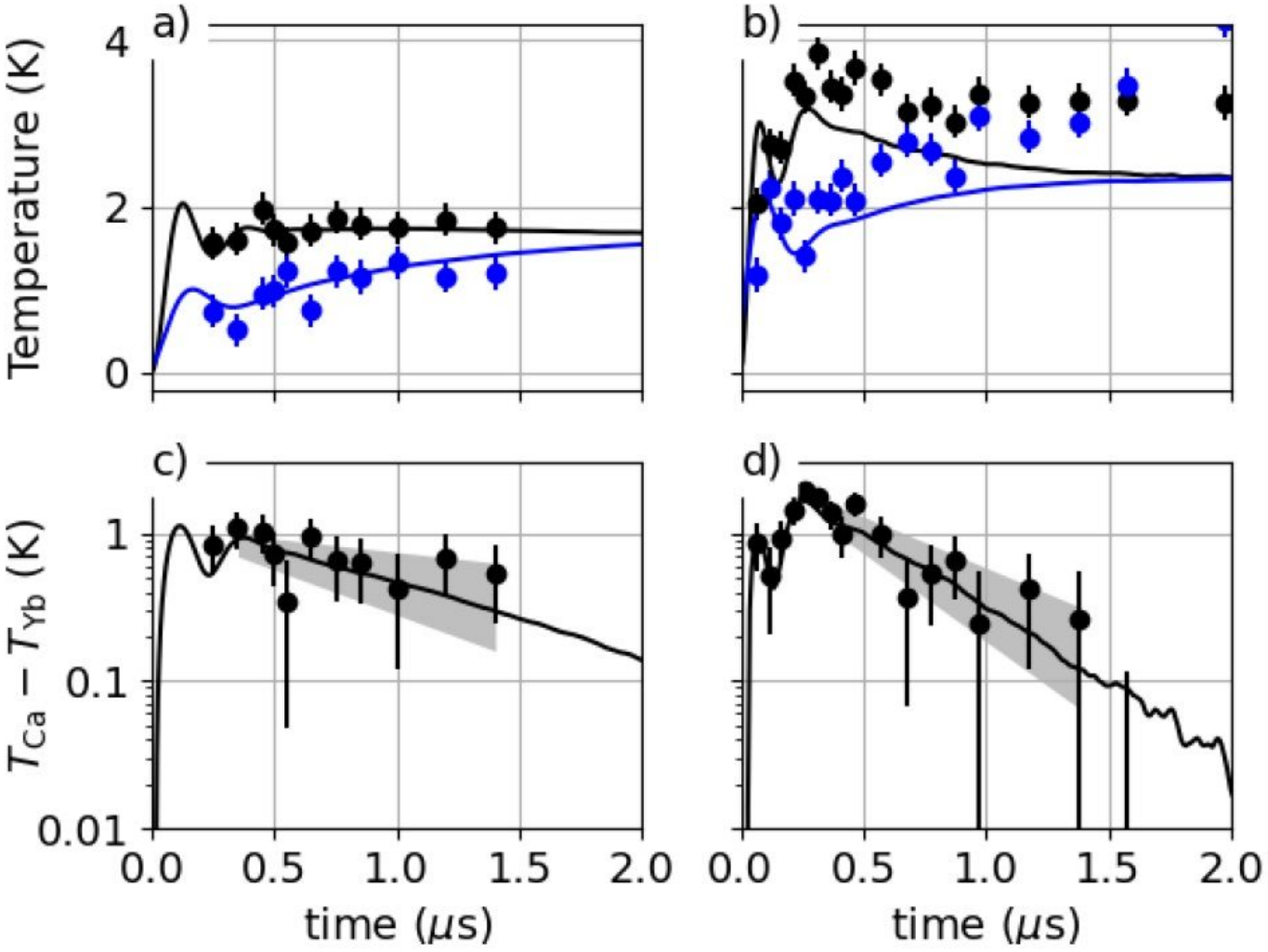

Figure 3

Temperature vs. time for two UNP configurations. (See Manuscript file for full figure caption)

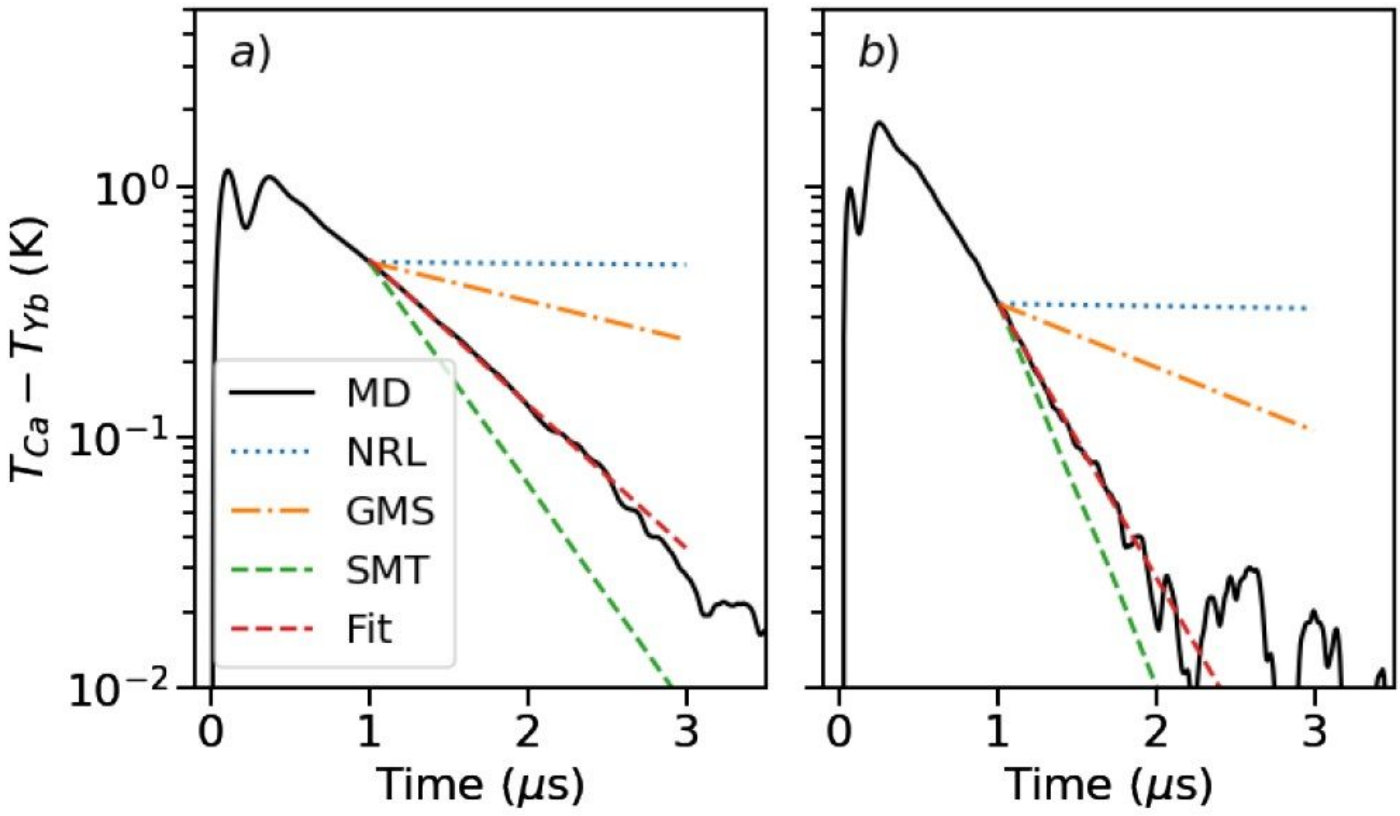

Figure 4

Semilog plot of the temperature difference (See Manuscript file for full figure caption)